

RECALIBRATION OF PAGEL'S METHOD FOR H II REGIONS CONSIDERING THE THERMAL STRUCTURE, THE IONIZATION STRUCTURE, AND THE DEPLETION OF O INTO DUST GRAINS

María A. Peña-Guerrero,²¹

guerrero@astro.unam.mx

Antonio Peimbert¹

antonio@astro.unam.mx

and

Manuel Peimbert¹

peimbert@astro.unam.mx

ABSTRACT

Using a sample of 28 H II regions from the literature with measured temperature inhomogeneity parameter, t^2 , we present a statistical correction to the chemical abundances determined with the $T_e(4363/5007)$ method. We used the t^2 values to correct the oxygen gaseous abundances and consider the oxygen depletion into dust to calculate the total abundances for these objects. This correction is used to obtain a new calibration of Pagel's strong-line method, R_{23} , to determine oxygen abundances in H II regions. Our new calibration simultaneously considers the temperature structure, the ionization structure, and the fraction of oxygen depleted into dust grains. Previous calibrations in the literature have included one or two of these factors; this is the first time all three are taken into account. This recalibration conciliates the systematic differences among the temperatures found from different methods. We find that the total correction due to thermal inhomogeneities and dust depletion amounts to an increase in the

¹Instituto de Astronomía, Universidad Nacional Autónoma de México, Apdo. Postal 70-264, México 04510 D.F., Mexico

²Currently at Space Telescope Science Institute, 3700 San Martin Drive, Baltimore, MD 21218, USA; pena@stsci.edu

O/H ratio of H II regions by factors of 1.7 to 2.2 (or 0.22 to 0.35 dex). This result has important implications in various areas of astrophysics such as the study of the higher end of the initial mass function, the star formation rate, and the mass-metallicity relation of galaxies, among others.

Subject headings: galaxies: abundances – H II regions galaxies: ISM – H II regions regions – H II regions ISM: abundances

1. Introduction

The study of physical conditions of H II regions is a fundamental tool to constrain models of nucleosynthesis of massive stars, galactic chemical evolution, and the chemical evolution of the Universe. In the same way, the study of the chemical composition of metal-poor H II regions is crucial for the understanding of the primordial chemical composition of the Universe. Most of these studies have been done using abundances obtained from the so called direct method, which assumes a homogeneous temperature throughout the whole volume of the object and then uses this temperature to determine abundances of all available ions; this temperature is commonly obtained from the [O III] collisionally excited line ratio $\lambda\lambda 4363/(4959+5007)$; hereafter we will call this procedure the $T_e(4363/5007)$ method.

Unfortunately, the simplification of the thermal structure of H II regions implied by the $T_e(4363/5007)$ method, yields lower abundances than those obtained with other methods. For example: (i) the O/H abundances derived from recombination lines, (ii) the O/H abundances derived by comparing the nebular lines with photoionization models, and (iii) the comparison of the O/H nebular abundances (including gas and dust), with those derived from B stars and young F and G stars (e.g. Bensby & Feltzing 2006; Kewley & Ellison 2008; Przybilla et al. 2008; Peimbert & Peimbert 2011; Simón-Díaz & Stasińska 2011; Nieva, & Przybilla 2012). The abundances derived from these three different methods are consistent within the errors. The abundances obtained through collisionally excited lines corrected for the presence of thermal inhomogeneities are consistent with the abundances obtained through other methods. For reviews on such issue see Peimbert & Peimbert (2011) and López-Sánchez et al. (2012).

Abundances obtained with the $T_e(4363/5007)$ method are underestimated because the temperature used in the determination process is assumed to be uniform. In the presence of either local or global thermal inhomogeneities, collisionally excited lines will be brighter in the hot regions while recombination lines will be brighter in the cool regions. This leads to choosing a temperature higher than the average and thus to assume that less oxygen (and

more hydrogen), than the amount that is actually present, is needed in order to reproduce the observed line intensities. For this reason, these abundances should be corrected for the presence of thermal inhomogeneities before being used to calibrate any strong-line indicator.

Pagel et al. (1979) were the firsts to introduce the R_{23} versus $12+\log(\text{O}/\text{H})$ diagram (from here on, this diagram will be referred to as the $R_{23}-\text{O}/\text{H}$ diagram). They found that the sum of the intensities of nebular oxygen with respect to $\text{H}\beta$, $I([\text{O II}] 3727) + I([\text{O III}] 4959+5007)/I(\text{H}\beta)$, varied smoothly with the total oxygen abundance and proposed to use what is now known as R_{23} , O_{23} , or Pagel’s method to determine the chemical abundances of objects where no auroral lines could be observed and, hence, no temperature could be determined. At present, more than a dozen strong-line indicators have been proposed; of them, the most studied is R_{23} (e.g. Stasińska 2006; Kewley & Ellison 2008; López-Sánchez et al. 2012). These strong-line indicators can be calibrated using well known abundance determinations such as the ones based on the $T_e(4363/5007)$ method or from fitting lines with numerical photoionization models.

The quality of the abundances derived with the $T_e(4363/5007)$ method, strongly depends on the validity of the assumption of constant temperature over the observed value. In the presence of large thermal inhomogeneities, the $T_e(4363/5007)$ method will underestimate abundances since the temperature dependence of the intensity of collisionally excited lines (such as $[\text{O III}] \lambda\lambda 4363, 4959, \text{ and } 5007$) is very different from that of the recombination line $\text{H}\beta$. The intensity of collisionally excited lines is proportional to $I \propto T_e^{-1/2} \times \exp(-\Delta E/kT_e)$, while the intensity of $\text{H}\beta$ is proportional to $I \propto T_e^{-0.87}$, where T_e is the local electron temperature, k is the Boltzmann constant, and ΔE is the collisional energy required to excite the line. As an alternative to avoid the problem of the large temperature dependence of collisionally excited lines, recombination lines can be used to determine abundances and calibrate the $R_{23}-\text{O}/\text{H}$ diagram because they have a temperature dependence given approximately by $I \propto T_e^{-1}$. For recombination line to $\text{H}\beta$ ratios, the temperature dependence almost cancels out, whereas for collisionally excited line to $\text{H}\beta$ ratios the temperature dependence does not cancel out. Some work has been done in the upper branch of the diagram using recombination lines, however, these faint lines can only be observed in metal-rich objects.

The discrepancy between abundances determined using recombination lines and collisionally excited lines is called the abundance discrepancy factor, ADF, problem. Typical values for H II regions lie in the 1.5 to 3 range (Peimbert et al. 1993, 2005; García-Rojas & Esteban 2007; Peimbert et al. 2007; Esteban et al. 2009, and references therein). There have been two major explanations for this discrepancy: (i) high metallicity inclusions that will create cool high density regions surrounded by hot low density regions (e.g. Tsamis & Péquignot 2005), and (ii) thermal inhomogeneities in a chemically homogeneous medium that are caused

by various physical processes such as shadowed regions, advancing ionization fronts, shock waves, magnetic reconnection, etc. (e.g. Peimbert & Peimbert 2011). Since the densities determined from oxygen recombination lines correlate very well with the [Cl III] densities (Peimbert & Peimbert 2005), we prefer the second explanation.

In Section 2 we discuss the corrections due to thermal inhomogeneities and due to the fraction of O depleted into dust grains. In Section 3 we present a quantitative correction to the $T_e(4363/5007)$ method, this correction is applied to the R_{23} method in Section 4. In Section 5 we discuss the relation between the O^{++} fraction and the intensity of the [O II] and [O III] nebular lines. Finally, in Section 6 we present the conclusions.

2. Temperature Inhomogeneities and Dust

The formalism to study the chemical abundances in the presence of thermal inhomogeneities was introduced by Peimbert (1967) and Peimbert & Costero (1969), where the parameter that characterizes such thermal inhomogeneities was defined as t^2 . In these works it was recognized that thermal inhomogeneities would produce systematic differences in temperatures determined from different methods, and that abundances determined with each one of those temperatures would also present systematic differences. The abundances determined using the $T_e(4363/5007)$ method were approximately a factor of 2.5 lower than those determined using the same collisionally excited line intensities including the effect of thermal inhomogeneities.

There are several ways to obtain a t^2 value, six of them are discussed in Peimbert & Peimbert (2011). These are based on the comparison of: (i) the O^{++} abundances obtained using [O III] lines versus abundances obtained using O II lines; (ii) the temperature derived from He I lines versus the temperatures derived from [O II] and [O III] lines; (iii) the temperatures derived from the ratio of the Balmer and Paschen continua to the Balmer line intensities versus the temperatures derived from [O II] and [O III] lines; (iv) the C^{++} abundances derived using [C III] and C III] lines versus abundances obtained from C II lines; (v) 1.5×10^6 columnar temperatures determined from a high spatial resolution map of the Orion nebula (O’Dell et al. 2003); and (vi) the calibrations of the R_{23} method using observations versus those using photoionization models. In all cases, the t^2 values are consistent with each other, which implies that those objects are chemically homogeneous. The first two methods are the most used to determine t^2 .

Independently of the effects of the thermal structure, there is an additional correction due to dust depletion that should be taken into account to determine abundances.

Esteban et al. (1998) found that the depletion of oxygen into dust grains in the Orion nebula amounted to a 0.08 dex correction in the O/H ratio; slightly higher estimates of this correction have been found in recent studies of the Orion nebula (Mesa-Delgado et al. 2009b; Simón-Díaz & Stasińska 2011). From the depletion of Mg, Si, and Fe in Galactic and extragalactic H II regions, Peimbert & Peimbert (2010) estimated an O/H correction ranging from 0.09 to 0.11 dex that increases with increasing O/H ratios. We have used the correction recommended by Peimbert et al. for all the objects of our sample; this corrections amounts to 0.11 dex for those objects whose gaseous oxygen abundance is $12+\log(\text{O}/\text{H}) > 8.3$, 0.10 dex for objects with $8.3 > 12+\log(\text{O}/\text{H}) > 7.8$, and 0.09 for those objects with $7.8 > 12+\log(\text{O}/\text{H})$.

3. Correction to the abundances derived with the $T_e(4363/5007)$ method

Due to the inconsistencies presented when comparing abundances obtained with the $T_e(4363/5007)$ method and those obtained with, recombination lines, photoionization models, and using abundances of recently formed stars; it is clear that abundances derived from the $T_e(4363/5007)$ method are systematically underestimated. This needs to be corrected by considering the thermal structure of the object and the fraction of oxygen depleted into dust grains.

Table 1 lists the sample we used to correct the $T_e(4363/5007)$ method. The sample consists on six H II galaxies, eight Galactic H II regions, and 14 extragalactic H II regions. This total of 28 objects were gathered from the literature and, in each of them, at least one value of t^2 was obtained. For the cases where there was more than one t^2 value we took the one presented as average or the one from the brightest observed region.

Based on detailed analysis presented in the literature it follows that the total oxygen abundance should be higher due to the effects of the thermal structure on the emitted spectra (e.g. Peimbert 1967; Peimbert & Costero 1969; Peimbert et al. 2000; Peimbert 2003; García-Rojas et al. 2004; Esteban et al. 2005; Peimbert et al. 2007; Esteban et al. 2009; Peimbert & Peimbert 2011; Peña-Guerrero et al. 2012; Peimbert et al. 2012) and that the fraction of O depleted into dust grains should be taken into account (Peimbert & Peimbert 2010, see also section 2). We expect the magnitude of these effects to depend on the oxygen abundance and, possibly, on the oxygen excitation degree. In order to take these factors into account, we considered that the abundances derived from the $T_e(4363/5007)$ method should be corrected with a function f dependent on the oxygen ionization degree and on the oxygen abundance determined from the $T_e(4363/5007)$ method, $(\text{O}/\text{H})_{4363/5007}$:

$$(\text{O}/\text{H})_{\text{CALM}} = (\text{O}/\text{H})_{4363/5007} + f(P, (\text{O}/\text{H})_{4363/5007}), \quad (1)$$

where CALM stands for Corrected Auroral Line Method. Throughout this paper all oxygen abundances are given in units of $12+\log(\text{O}/\text{H})$.

As a first approximation to the function f , we decided to use a linear correction of the form

$$f(P, (\text{O}/\text{H})_{4363/5007}) = C_1 + C_2 \times (\text{O}/\text{H})_{4363/5007} + C_3 \times P + C_4 \times P \times (\text{O}/\text{H})_{4363/5007}, \quad (2)$$

where C_1 , C_2 , C_3 , and C_4 are constants.

All abundances determined for our sample were corrected for (i) the presence of thermal inhomogeneities and (ii) the fraction of oxygen depleted into dust grains. We have found that the difference between these corrected abundances and those determined with the $T_e(4363/5007)$ method lie in the 0.16 to 0.40 dex range.

We found very little dependence with oxygen degree of ionization: C_3 and C_4 are 0.010 and 0.0002, respectively. Since the dependence with ionization degree is small and consistent with zero we will ignore it. Figure 1 presents the oxygen abundance correction dependence with oxygen abundance for the objects of our sample. The best fit is obtained with C_1 and C_2 equal to -0.375 and 0.0825 , respectively:

$$f(P, (\text{O}/\text{H})_{4363/5007}) = f((\text{O}/\text{H})_{4363/5007}) = 0.0825(\text{O}/\text{H})_{4363/5007} - 0.375; \quad (3)$$

this implies a corrected oxygen abundance:

$$(\text{O}/\text{H})_{\text{CALM}} = 1.0825(\text{O}/\text{H})_{4363/5007} - 0.375. \quad (4)$$

The points in Figure 1 show considerable dispersion; this is not surprising, because (i) the errors in the determination of each t^2 value are large and (ii) the true value of t^2 for each object depends on the details of the object (see Figure 4 of Peimbert et al. 2012). To test for the statistical significance of this correlation we calculated a Spearman’s correlation statistic of $\rho = 0.3685$, this suggests that the correlation is real with 95% confidence. When comparing the dispersion with the uncertainties on the oxygen abundance determinations for this sample we calculated $\chi^2 = 60.28$; showing that about half of this dispersion comes from the uncertainties of the determination of t^2 ; meaning that approximately half of the dispersion comes from the unique physical conditions of each object.

4. Recalibration of the R_{23} Abundance Determination Method

R_{23} is now being widely used to determine abundances in objects with low intrinsic brightness or objects with low to intermediate redshift (z up to 1). The R_{23} method remains

one of the most popular strong line indicators because (i) it is based directly on oxygen lines, (ii) it includes lines from the 2 relevant ionization stages, (iii) the lines it uses are the most intense for most H II regions, and (iv) these lines lie in the blue part of the spectrum and can be observed from the ground for higher redshifts than other methods.

Unfortunately, the curve in the $R_{23} - \text{O}/\text{H}$ diagram is double valued (see Figure 2); this occurs because: at low metallicities, the main cooler in H II regions is the hydrogen atom; with increasing element abundances, the cooling due to oxygen nebular lines increases, hence, the value of R_{23} increases reaching a maximum value of $R_{23} \approx 10$ when $12 + \log(\text{O}/\text{H})_{\text{ISM}} \approx 8.4$; then, at higher metallicities, the IR [O III], IR [Ne II], and optical [N II] lines begin to dominate the cooling so that the total value of R_{23} decreases as the metallicity increases (Van Zee et al. 1998).

Also, there is a noticeable dependence on the oxygen ionization degree (e.g. McGaugh 1991; Kewley & Dopita 2002). In a series of articles Pilyugin (2000, 2001) and Pilyugin & Thuan (2005), presented an analytic family of curves for each branch of the $R_{23} - \text{O}/\text{H}$ diagram. This family of curves depends on the oxygen excitation degree across the object; defining the P parameter as the observable oxygen excitation ratio, $P = ([\text{O III}] 4959 + 5007) / ([\text{O II}] 3727 + [\text{O III}] 4959 + 5007)$, and presenting two equations to determine the upper and lower branch abundances as a function of $(\text{O}/\text{H})_{\text{P}} = f(P, R_{23})$. This calibration is based on abundances determined using the $T_e(4363/5007)$ method.

Unfortunately, depending on the calibration, resultant O/H values can vary by as much as 0.6 dex (Peimbert et al. 2007; Kewley & Ellison 2008). This large dispersion in the calibrations mainly comes from what was chosen to be adjusted: (i) the theoretical intensities given by photoionization models, (ii) abundances derived from the $T_e(4363/5007)$ method, or (iii) abundances derived from observations of oxygen recombination lines. The lowest determinations for the gaseous oxygen abundances are those that come from using the $T_e(4363/5007)$ method, therefore they require the correction due to thermal inhomogeneities; additionally, to obtain the total oxygen abundances, a correction of ~ 0.10 dex —due O depletion into dust grains— is required.

We find that, among all the calibrations of the $R_{23} - \text{O}/\text{H}$ diagram available in the literature, the one presented by Pilyugin & Thuan (2005) is the most adequate for this work since it explicitly includes the oxygen ionization degree through the P parameter.

The calibration of Pilyugin & Thuan (2005), $(\text{O}/\text{H})_{\text{P}}$, used abundances that were determined with the $T_e(4363/5007)$ method; hence, abundances are underestimated but this allows us to use equation 4 to correct them since $(\text{O}/\text{H})_{\text{P}}$ has abundances determined with the $T_e(4363/5007)$ method at its core. We can determine oxygen abundances from a recalibration

of the R_{23} method, $(\text{O}/\text{H})_{\text{RRM}}$, by substituting $(\text{O}/\text{H})_{\text{RRM}}$ and $(\text{O}/\text{H})_{\text{P}}$ in place of $(\text{O}/\text{H})_{\text{CALM}}$ and $(\text{O}/\text{H})_{4363/5007}$ into equation (4). We take $(\text{O}/\text{H})_{\text{P}}$ from equation [22] and [24] of Pilyugin and Thuan for the upper and lower branches, respectively, to obtain two recalibrated families of curves that now simultaneously consider the thermal structure, the ionization structure, and the depleted fraction of O into dust grains. The oxygen abundance for the upper branch (which shifted from $12+\log(\text{O}/\text{H})_{\text{P}} \geq 8.25$ up to $12+\log(\text{O}/\text{H})_{\text{RRM}} \geq 8.55$), can be estimated from:

$$\begin{aligned} (\text{O}/\text{H})_{\text{RRM}} &= \left(\frac{R_{23} + 726.1 + 8.42P + 327.5P^2}{85.96 + 82.76P + 43.98P^2 + 1.793R_{23}} \right) 1.0825 - 0.375 \\ &= \frac{R_{23} + 1837 + 2146P + 850P^2}{209.5 + 201.7P + 107.2P^2 + 4.37R_{23}}, \end{aligned} \quad (5)$$

while the oxygen abundance for the lower branch (which shifted from $12+\log(\text{O}/\text{H})_{\text{P}} \leq 8.00$ up to $12+\log(\text{O}/\text{H})_{\text{RRM}} \leq 8.29$), can be estimated from:

$$\begin{aligned} (\text{O}/\text{H})_{\text{RRM}} &= \left(\frac{R_{23} + 106.4 + 106.8P - 3.40P^2}{17.72 + 6.60P + 6.95P^2 - 0.302R_{23}} \right) 1.0825 - 0.375 \\ &= \frac{R_{23} + 90.73 + 94.58P - 5.26P^2}{14.81 + 5.52P + 5.81P^2 - 0.252R_{23}}. \end{aligned} \quad (6)$$

Figure 2 shows these recalibrations of the upper and lower branches for different oxygen ionization degrees, while Figure 3 compares the calibration presented in this work and that of Pilyugin & Thuan (2005) to the data from Table 1.

5. The O^{++} fraction

Something missing when using the P parameter is a quantitative connection with the O^{++} fraction in the nebulae. We will define the O^{++} ionization degree as:

$$\text{OID} = \frac{\int n_e n(\text{O}^{++}) dr}{\int n_e n(\text{O}^+ + \text{O}^{++}) dr}. \quad (7)$$

Since there is a tight relationship between the parameter P and the O^{++} ionization degree (see Figure 4), the fraction of O^{++} in the object can be estimated through the the following equation:

$$\text{OID} = 0.9821P - 0.0048. \quad (8)$$

This equation allows us to statistically estimate the O^{++} ionization degree directly from the observable P without having to make a lengthy analysis of the ionic abundances. It should be noted that while this relation shows no significant bias with the O/H ratio, more points are needed to confirm the lack of bias or to estimate the relevance of the oxygen abundance in this correlation.

6. Conclusions

We used a sample of 28 H II regions obtained from the literature, with t^2 values ranging from 0.020 to 0.120, to present an important correction to the abundances derived with the $T_e(4363/5007)$ method, as well as a recalibration of Pagel’s strong-line method, R_{23} to determine chemical abundances. Both, the correction and the recalibration consider the thermal and ionization structure of the object, as well as the fraction of oxygen depleted into dust grains. We found that the differences between the corrected abundances and those determined with the $T_e(4363/5007)$ method lie in the 0.22 to 0.35 dex range.

Almost all previous calibrations of the $R_{23} - O/H$ diagram in the literature have considered a homogeneous temperature throughout the object. The recalibration presented in equations 5 and 6, is the first to simultaneously consider the thermal structure of the photoionized object, the ionization structure, and the correction due to the fraction of oxygen depleted into dust grains. This recalibration is particularly useful for objects with low to intermediate redshifts (up to $z \approx 1$).

We find that the O^{++} ionization degree shows a surprisingly almost one-to-one relation with the parameter P , thus ensuring that a calibration which considers P is directly considering the oxygen ionization structure of the object.

Given that all strong-line indicators attempt to determine the total oxygen abundance as means of estimating the heavy element content, and that all the observational calibrations have been done using abundances determined with the $T_e(4363/5007)$ method, the oxygen correction presented in this paper should be used to recalibrate other strong-line indicators in the literature.

The up-shifting of the family of curves in the $R_{23} - O/H$ diagram found in this work, has important consequences in various areas of astrophysics such as the determination of: initial mass functions, star formation rates, luminosity functions, yields, radial metallicity gradients of spiral galaxies, and chemical evolution models of the Universe.

We are grateful to an anonymous referee for a careful reading of the manuscript and

several useful suggestions. MAPG and AP received partial support from UNAM (grant PAPIIT 112911) and AP and MP received partial support from CONACyT (grant 129753).

REFERENCES

- Bensby, T., & Feltzing, S. 2006, *MNRAS*, 367, 1181
- Esteban, C., Bresolin, F., Peimbert, M., et al. 2009, *ApJ*, 700, 654
- Esteban, C., García-Rojas, J., Peimbert, M., et al. 2005, *ApJ*, 618, L95
- Esteban, C., Peimbert, M., García-Rojas, J., et al. 2004, *MNRAS*, 355, 229
- Esteban, C., Peimbert, M., Torres-Peimbert, S., & Escalante, V. 1998, *MNRAS*, 295, 401
- Esteban, C., Peimbert, M., Torres-Peimbert, S., & Rodríguez, M. 2002, *ApJ*, 581, 241
- García-Rojas, J., & Esteban, C. 2007, *ApJ*, 670, 457
- García-Rojas, J., Esteban, C., Peimbert, A., et al. 2005, *MNRAS*, 362, 301
- García-Rojas, J., Esteban, C., Peimbert, A., et al. 2007, *RevMexAA*, 43, 3
- García-Rojas, J., Esteban, C., Peimbert, M., et al. 2006, *MNRAS*, 368, 253
- García-Rojas, J., Esteban, C., Peimbert, M., et al. 2004, *ApJ*, 153, 501
- Izotov, Y. I., & Thuan, T. X. 1999, *ApJ*, 511, 639
- Izotov, Y. I., Thuan, T. X., & Lipovetsky, V. A. 1997, *ApJS*, 108, 1
- Kewley, L. J., & Dopita, M. A. 2002, *ApJS*, 142, 35
- Kewley, L. J., & Ellison, S. 2008, *ApJ*, 681, 1183
- López-Sánchez, A. R., Dopita, M. A., Kewley, L., Zahid, H. J., Nicholls, D. C., & Scharw'acheter, J. 2012, *asto-ph.CO 1203.5021v1*
- López-Sánchez, A. R., Esteban, C., García-Rojas, J., et al. 2007, *ApJ*, 656, 168
- McGaugh, S. S. 1991, *ApJ*, 380, 140
- Mesa-Delgado, A., Esteban, C., García-Rojas, J., et al. 2009, *MNRAS*, 395, 855
- Nieva, M. -F. & Przybilla, N. 2012, *A&A*, 539, A143

- O'Dell, C. R., Peimbert, M., & Peimbert, A. 2003, *AJ*, 125, 2590
- Pagel, B. E. J., Edmunds, M. G., Blackwell, D. E., Chun, M. S., & Smith G. 1979, *MNRAS*, 189, 95-113
- Peimbert, A. 2003, *ApJ*, 584, 735
- Peimbert, A., & Peimbert, M. 2005, *RevMexAA(SC)*, 23, 9
- Peimbert, A., & Peimbert, M. 2010, *ApJ*, 724, 791
- Peimbert, A., Peimbert, M., & Ruiz, M. T. 2005, *ApJ*, 634, 1056
- Peimbert, A., Peña-Guerrero, M. A., & Peimbert, M. 2012, *ApJ*, in press
- Peimbert, M. 1967, *ApJ*, 150, 825
- Peimbert, M., & Costero, R. 1969, *Bol. Obs. Tonantzintla y Tacubaya*, 5, 3
- Peimbert, M., & Peimbert, A. 2011, *RevMexAA(SC)*, 39, 1
- Peimbert, M., Peimbert, A., Esteban, C., et al. 2007, *RevMexAA(SC)*, 29, 72
- Peimbert, M., Peimbert, A., & Ruiz, M. T. 2000, *ApJ*, 541, 688
- Peimbert, M., Peimbert, A., Ruiz, M. T., & Esteban, C. 2004, *ApJS*, 150, 431
- Peimbert, M., Storey, P. J., & Torres-Peimbert, S. 1993, *ApJ*, 414, 626
- Peña-Guerrero, M. A., Peimbert, A., Peimbert, M., & Ruiz, M. T. 2012, *ApJ*, 746, 115
- Pilyugin, L. S. 2000, *A&A*, 362, 325
- Pilyugin, L. S. 2001, *A&A*, 369, 594
- Pilyugin, L. S., & Thuan, T. Z. 2005, *AJ*, 631, 231-243
- Przybilla, N., Nieva, M. -F., & Butler, K. 2008, *ApJ*, 688, L103
- Simón-Díaz, S., & Stasińska, G. 2011, *A&A*, 526, A48
- Stasińska, G. 2006, *A&A*, 454, L127
- Tsamis, Y. G., & Péquignot, D. 2005, *MNRAS*, 364, 687
- Van Zee, L., Salzer, J. J., Haynes, M. P., O'Donoghue, A. A., & Balonek, T. J. 1998, *ApJ*, 116, 2805

Table 1. H II region data

Object	Type ^a	$T_e[\text{O III}]$	t^2	$\log(R_{23})$	P	$\frac{\text{O}^{++}}{\text{O}^+ + \text{O}^{++}}$	O/H ^b	O/H ^c	References
Upper branch									
NGC 3576	GR	8500±50	0.038±0.009	0.78	0.78	0.67	8.56	8.92	1
M16	GR	7650±250	0.039±0.006	0.59	0.28	0.25	8.50	8.90	2
M17	GR	8950±380	0.033±0.005	0.73	0.83	0.83	8.52	8.88	3
M8	GR	8090±140	0.040±0.004	0.53	0.38	0.28	8.51	8.85	3
H1013	XR	7370±630	0.037	0.42	0.49	0.49	8.45	8.84	4
NGC 595	XR	7450±330	0.036	0.51	0.37	0.44	8.45	8.80	4
M20	GR	7800±300	0.029±0.007	0.60	0.20	0.17	8.53	8.79	2
Orion	GR	8300±40	0.028±0.006	0.77	0.86	0.83	8.51	8.79	5, 6
NGC 3603	GR	9060±200	0.040±0.008	0.89	0.92	0.93	8.46	8.78	2
K932	XR	8360±150	0.033	0.72	0.72	0.79	8.41	8.73	4
NGC 2403	XR	8270±210	0.039	0.59	0.66	0.67	8.36	8.72	4
NGC 604	XR	8150±160	0.034±0.015	0.60	0.71	0.71	8.38	8.71	4
S 311	GR	9000±200	0.038±0.007	0.72	0.32	0.31	8.39	8.67	7
NGC 5447	XR	9280±180	0.032	0.85	0.78	0.86	8.35	8.63	4
30 Doradus	XR	9950±60	0.033±0.005	0.90	0.85	0.85	8.33	8.61	8
NGC 5461	XR	8470±200	0.027±0.012	0.71	0.80	0.77	8.41	8.60	4, 9
NGC 5253	HIIG	11960±290	0.072±0.027	0.96	0.85	0.78	8.18	8.56	10
Transition zone									
NGC 6822-V	XR	13000±1000	0.076±0.018	0.91	0.88	0.89	8.08	8.45	11
NGC 5471	XR	14100±300	0.082±0.030	0.93	0.75	0.78	8.03	8.33	9
NGC 456	XR	12165±200	0.067±0.013	0.83	0.78	0.80	7.99	8.33	12
Lower branch									
NGC 346	XR	13070±50	0.022±0.008	0.92	0.88	0.69	8.07	8.23	13, 14

Table 1—Continued

Object	Type ^a	T_e [O III]	t^2	$\log(R_{23})$	P	$\frac{O^{++}}{O^++O^{++}}$	O/H ^b	O/H ^c	References
NGC 460	XR	12400±450	0.032±0.032	0.81	0.62	0.56	7.96	8.19	12
NGC 2363	XR	16200±300	0.120±0.010	0.92	0.97	0.97	7.76	8.14	4
TOL 2146 – 391	HIIG	15800±170	0.107±0.034	0.91	0.92	0.86	7.79	8.09	15
TOL 0357 – 9315	HIIG	14870±230	0.029±0.064	0.93	0.93	0.87	7.90	8.12	15
Haro 29	HIIG	16050±100	0.019±0.007	0.91	0.91	0.88	7.87	8.05	13, 16
SBS 0335–052	HIIG	20500±200	0.021±0.007	0.67	0.93	0.93	7.35	7.60	13, 17
I Zw 18	HIIG	19060±610	0.024±0.006	0.47	0.86	0.90	7.22	7.41	13, 17

References.— (1) García-Rojas et al. (2004); (2) García-Rojas et al. (2006); (3) García-Rojas et al. (2007); (4) Esteban et al. (2009); (5) Esteban et al. (2004); (6) O’Dell et al. (2003); (7) García-Rojas et al. (2005); (8) Peimbert (2003); (9) Esteban et al. (2002); (10) López-Sánchez et al. (2007); (11) Peimbert et al. (2005); (12) Peña-Guerrero et al. (2012); (13) Peimbert et al. (2007); (14) Peimbert et al. (2000); (15) Peimbert et al. (2012); (16) Izotov et al. (1997); (17) Izotov & Thuan (1999).

^aGR=Galactic region, XR=Extragalactic region, HIIG= H II Galaxy.

^bGaseous O abundance with homogeneous temperature, $t^2=0.000$. In units of $12+\log(O/H)$.

^cTotal O abundance with thermal inhomogeneities, $t^2>0.000$, including the correction due to depletion of O into dust grains. In units of $12+\log(O/H)$.

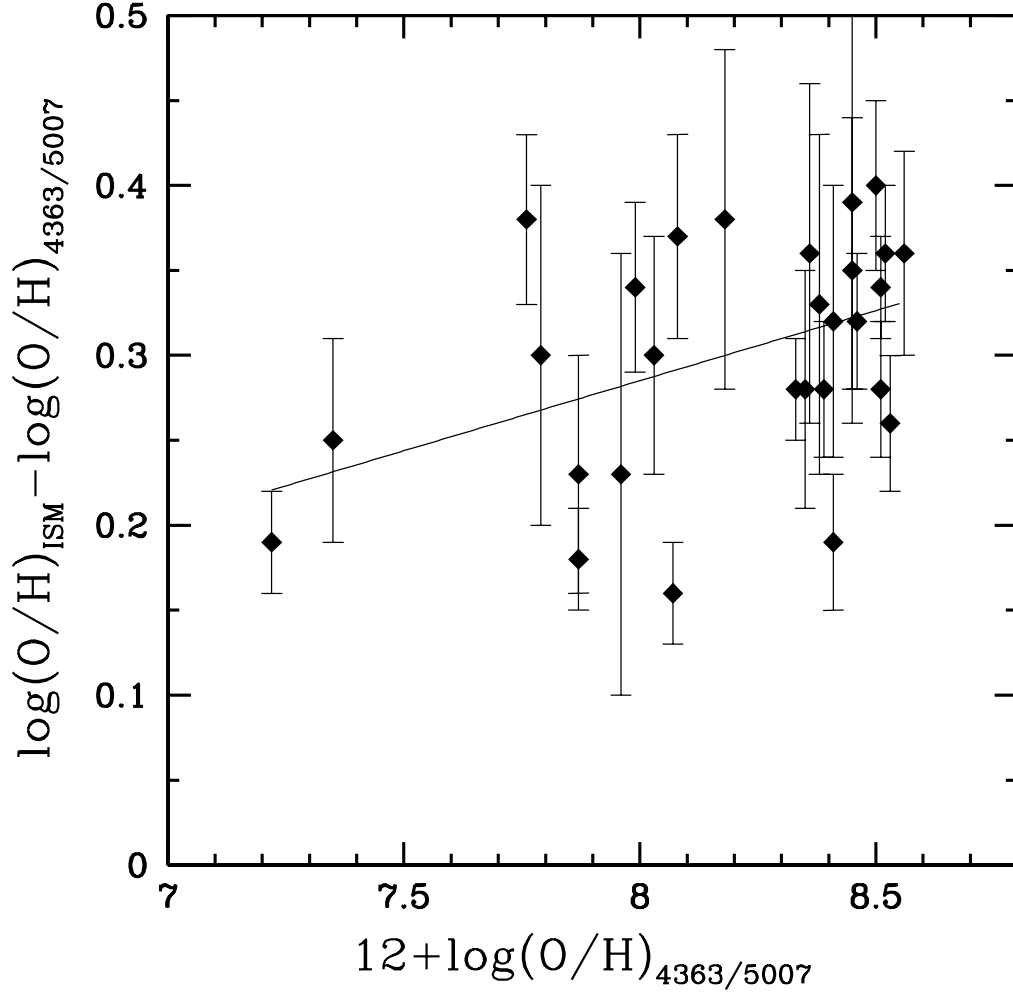


Fig. 1.— Plot of the abundances obtained with the $T_e(4363/5007)$ method, versus the difference in dex between the corrected abundances and those obtained with the $T_e(4363/5007)$ method. The line is the best linear fit to the objects presented in Table 1, $\log(O/H)_{\text{ISM}} - \log(O/H)_{4363/5007} = 0.0825 \times [12 + \log(O/H)_{4363/5007}] - 0.375$.

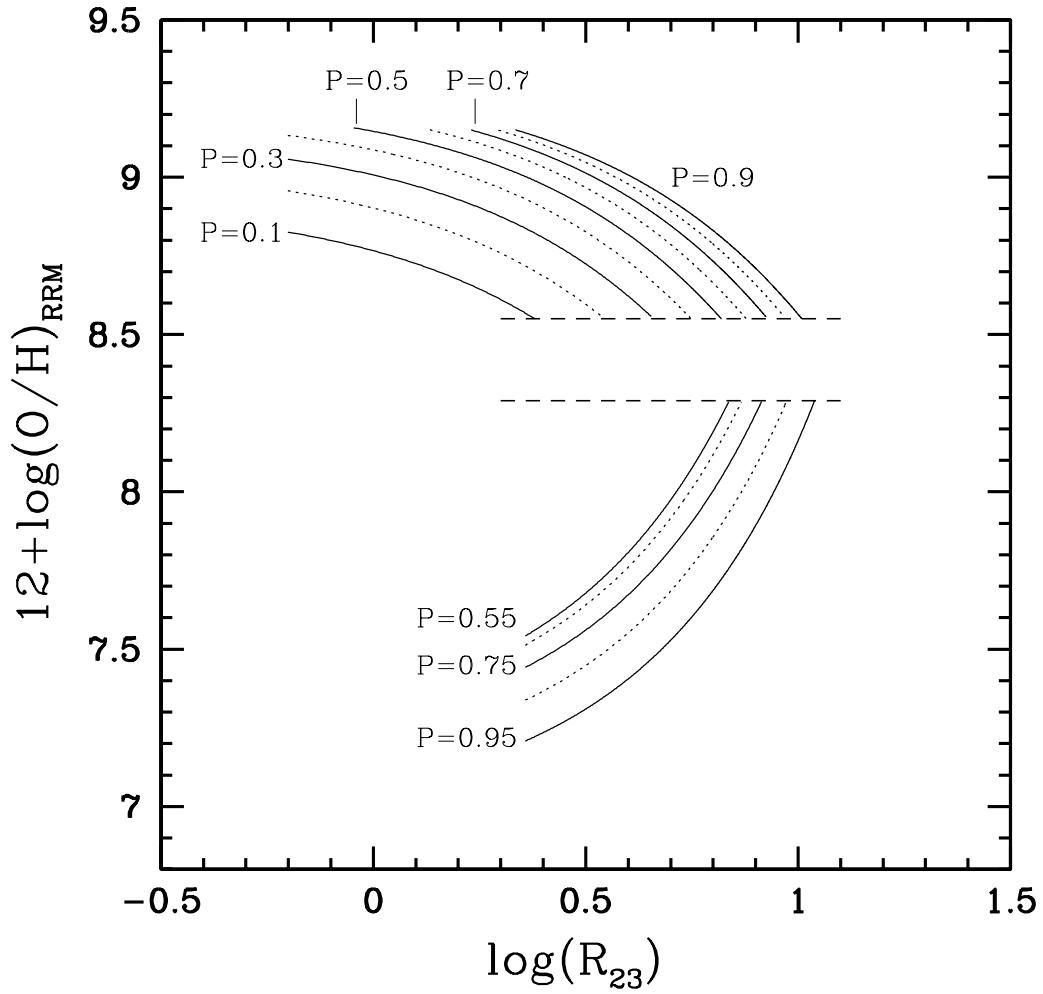


Fig. 2.— New calibration of the R_{23} Method from equations 5 and 6. For clarity, the solid P -valued curves have been labeled. The dashed horizontal lines indicate the transition zone between the upper and lower branches.

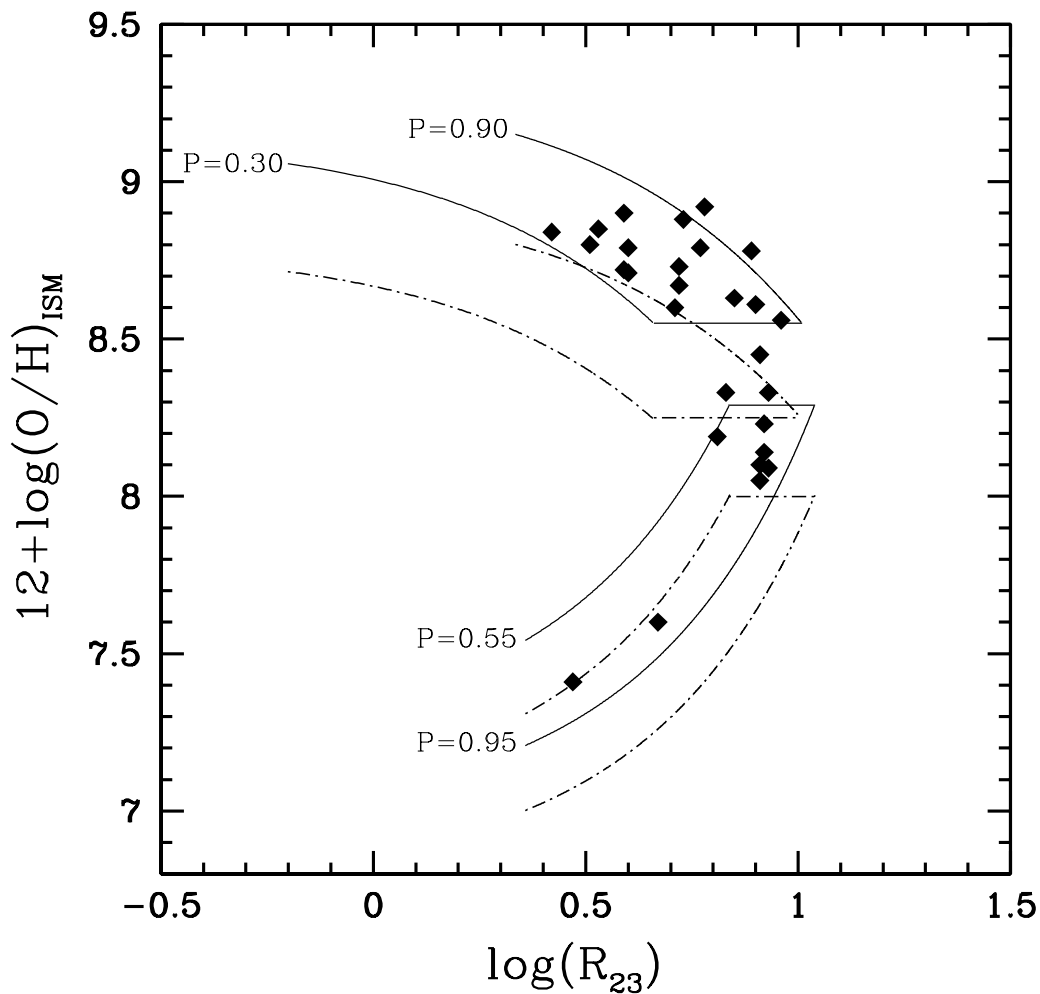


Fig. 3.— Plot of the oxygen abundance vs. R_{23} for the 28 objects from Table 1, where abundances were determined considering the presence of thermal inhomogeneities as well as the fraction of O depleted into dust grains. For comparison we present representative bands of the upper and lower branches for both nebular line calibrations, $(O/H)_{\text{RRM}}$ (solid black curves) and $(O/H)_{\text{P}}$ (point-dashed curves).

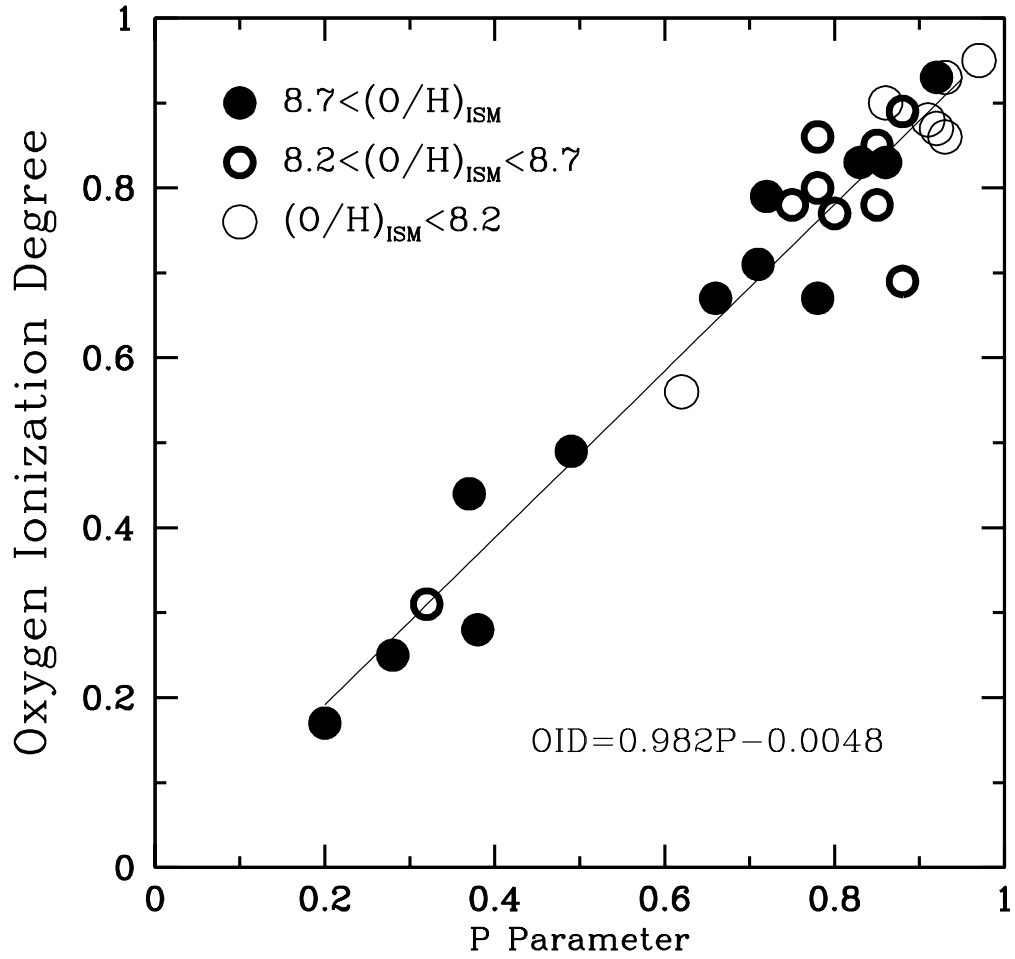


Fig. 4.— Linear relation found between the observational parameter P and the true O^{++} ionization degree. The objects used to obtain this relation are those listed in Table 1.